Global Circulation in an Axially Symmetric Shallow Water Model Forced by Equinoctial Differential Heating

ORI ADAM AND NATHAN PALDOR

Institute of Earth Sciences, The Hebrew University of Jerusalem, Jerusalem, Israel

(Manuscript received 19 November 2007, in final form 12 September 2008)

ABSTRACT

Solutions of an axially symmetric inviscid shallow-water model (SWM) on the earth forced by equinoctial differential heating are constructed using numerical integration of the time-dependent equations and analysis of their steady states. The study also maps the physical initial conditions and parameter values for which the solutions approach steady states at long times, demonstrating strong dependence of the SWM on initial conditions. The model admits states of uniform angular momentum, including superrotation, in the tropics and radiative equilibrium at high latitudes. The asymptotic properties of the subtropical jets and tropical fluxes are explicitly calculated and it is shown that all solutions of the previously studied nearly inviscid theories are particular solutions of the present theory. The model's results relate the location and intensity of the subtropical jet in the steady states to properties of the SWM on a sphere, such as the conservation of angular momentum. The exact form of the differential heating is secondary in determining these properties and its main role is to transform any initial state to the vicinity of the steady states.

When mass is assumed to be supplied to the fluid from an underlying motionless layer (this model is termed the 1½-SWM), the angular momentum in the tropics is not uniform (so the local Rossby number is smaller than 1), the height of the tropopause is nearly uniform there, the steady states do not depend on the initial conditions, and the zonal velocity vanishes on the equator. Accurate and simple estimates that are determined only by the value of a thermal Rossby number are derived in this case for the location and intensity of the subtropical jet.

1. Introduction

Axially symmetric models that describe the zonally averaged general circulation of the atmosphere are most relevant to the tropics where a weak Hadley circulation is produced even when large-scale eddies are suppressed. Poleward of the tropics, macroturbulent and moist momentum heat fluxes dominate those of the mean circulation and, therefore, significantly influence the circulation strength and width and the meridional profile of the subtropical jet. Macroturbulent and moist theory, however, must build upon axially symmetric theory as the latter represents an asymptotic limit of the former (Schneider 2006).

The scant data available in the 1960s (Lorenz 1967) pointed to the role that the tropical (Hadley) circulation plays in the horizontal poleward transport of energy and momentum. The first detailed numerical calculations of axially symmetric models of the circulation were done by Schneider and Lindzen (1977) and Schneider (1977), followed by Held and Hou (1980, hereafter HH80). The nearly-inviscid, simple steady-state theory of HH80 (for simplicity, HH80 theory) was shown by HH80 to provide an approximation to the numerically calculated steady states. The solutions at the rigid lid that marks the tropopause were constructed by assuming 1) an energetically closed upper branch in the tropics with uniform absolute angular momentum (hereafter referred to simply as angular momentum), 2) balanced wind, 3) negligible horizontal velocity at the earth's surface (where surface friction dominates the force balance), and 4) Newtonian cooling that relaxes toward radiative equilibrium. Subsequent studies of axially symmetric models in the limit of vanishing viscosity extended HH80 theory to off-equatorial heating (Lindzen and Hou 1988), more general steady meridional heating distributions (Hou and Lindzen 1992; Plumb and Hou 1992; Fang and Tung 1996), radiative–convective forcing (Satoh 1994), and time-dependent heating (Fang and Tung 1999).

Corresponding author address: Nathan Paldor, Institute of Earth Sciences, Admond Safra Campus, Givat Ram, The Hebrew University of Jerusalem, Jerusalem, 91904, Israel.
E-mail: nathan.paldor@huji.ac.il

DOI: 10.1175/2008JAS2685.1

While HH80 theory provided a great qualitative advance in dynamical meteorology, some ambiguity exists regarding the interpretation and validity of its predictions. First, in the inviscid limit (in which the width and strength of the Hadley circulation become independent of the value of the turbulent viscosity) the HH80 model becomes a barotropic layer that lies on top of a thin surface boundary layer (cf. Fig. A1 of Williams 2003). However, in HH80's simulation of the tropical circulation on earth the atmosphere in midlatitudes is highly baroclinic and sensitive to changes in the viscosity, which defies the nearly-inviscid assumption (Walker and Schneider 2005). Second, the assumption of a rigid lid that bounds the atmosphere from above inevitably introduces a spurious magnification of the wind there in some cases (Walker and Schneider 2005). Third, the inviscid paradigm of a tropical uniform angular momentum region and an extratropical radiative equilibrium region entails a discontinuity in the zonal wind at the boundary between these regions, which is not expected to exist in reality.

The shallow-water model (SWM) used in the present work relaxes both the need for adding viscosity to the governing equations and the existence of a rigid lid at the upper boundary, making it ideal for simulating inviscid dynamics (which the upper branch of the Hadley circulation is supposed to obey). The relative simplicity of the SWM allows one to obtain analytical solutions in particular cases while retaining the essential properties of the general circulation (e.g., Polvani and Sobel 2002; Shell and Held 2004).

The SWM describes the fluid dynamics in a thin isentropic layer in hydrostatic equilibrium and, as such, precludes diabatic dynamics that may be particularly relevant in midlatitudes where isentropic surfaces intersect the tropopause (Held and Phillips 1990). The large-scale balanced dynamics of the upper troposphere, however, have been shown to be captured in a succinct and simple manner by the concept of isentropic potential vorticity (Hoskins et al. 1985). Under such a representation, the midlatitude isentropic tropopause is associated with steep potential vorticity gradients. Such steep gradients are reproduced by isentropic models, implying that adiabatic motion significantly affects the shape of the tropopause (Ambaum 1997).

Plumb and Hou (1992) and Fang and Tung (1999) noted that the adjustment time required for an axially symmetric model to approach steady state is significantly longer than a season, which poses additional difficulties associated with numerical instabilities in long integrations. The SWM allows the inviscid equations to be integrated over very long times using negligible explicit numerical viscosities, thus enabling the study of the model's inviscid (Eulerian) steady states.

Using the angular momentum as a dynamic variable greatly simplifies the analysis of nonlinear dynamics on a rotating sphere in various settings, for example, Plumb and Hou (1992), inertial motion (Paldor 2001), equatorial crossing of tropical monsoon systems (Dvorkin and Paldor 1999), and Ekman transport (Paldor 2002). In the present work we analyze the nonlinear SWM on the rotating spherical earth and derive some constraints on its solutions by studying the evolution equation for angular momentum instead of merely applying its conservation as was done in some previous studies.

As pointed out by Fang and Tung (1996), in Eulerian flows the meridional distribution of the angular momentum is the solution of an initial value problem. Viscous steady flows, however, introduce an additional constraint whereby the angular momentum maximizes at the lower boundary. This property that follows from Hide's theorem for steady viscous flows [cf. HH80; for more details, Plumb and Hou(1992)] indicates that analytical results obtained for Eulerian flows differ from numerical results obtained in the limit of vanishing viscosity. Fang and Tung (1996) also note that, since the atmosphere is never in a steady state, it is not clear whether the relevant theory is Eulerian or nearly inviscid.

Recently, Walker and Schneider (2006) and Schneider (2006) showed that zonally and temporally averaged circulations of an idealized dry general circulation model (GCM) do not follow the predictions of nearly-inviscid theory except for special cases, stressing the need for an improved axially symmetric theory. This work is an attempt to construct such an axially symmetric model of the circulation on earth that contains few parameters (so it can be simply analyzed) and includes the solar differential heating. To this end we employ a SWM properly parameterized to include the solar differential heating, which satisfies the simplicity and clarity requirements and removes the rigid-lid assumption of the HH80 theory.

The layout of this work is as follows: the model is introduced and its steady states are analyzed in section 2. The time-dependent equations are integrated numerically in section 3, and the asymptotic states of the system at long times are solved for steady equinoctial forcing. In section 4 the physical nature of the forcing is studied by considering modifications of the forcing corresponding to different physical premises. The paper ends with a summary and discussion in section 5.

2. Model equations and steady states

a. Model equations

The equations of the SWM on a spherical earth (with radius a, latitude ϕ, and longitude λ coordinates) rotating

about its polar axis (frequency Ω but no centrifugal acceleration) with a source of mass (height) Q are given by (Gill 1982)

$$\frac{Dv}{Dt} = -\left(2\Omega + \frac{u}{a\cos\phi}\right)u\sin\phi - \frac{g}{a}\frac{\partial h}{\partial\phi}, \tag{1a}$$

$$\frac{Du}{Dt} = \left(2\Omega + \frac{u}{a\cos\phi}\right)v\sin\phi - \frac{g}{a\cos\phi}\frac{\partial h}{\partial\lambda}, \tag{1b}$$

and

$$\frac{\partial h}{\partial t} + \frac{1}{a\cos\phi}\left(\frac{\partial}{\partial\lambda}(hu) + \frac{\partial}{\partial\phi}(hv\cos\phi)\right) = Q, \tag{1c}$$

where

$$\frac{D}{Dt} = \frac{\partial}{\partial t} + \frac{u}{a\cos\phi}\frac{\partial}{\partial\lambda} + \frac{v}{a}\frac{\partial}{\partial\phi}$$

denotes the material (total, Lagrangian) derivative in spherical coordinates and where g is the gravitational constant, u and v denote the longitudinal and meridional velocity components, respectively, and h denotes the thickness of the atmosphere. The source Q on the right-hand side (rhs) of the continuity equation (1c) is associated with differential solar heating given by

$$Q = -\frac{h - h_f}{\tau} \tag{1d}$$

and

$$h_f = H_0 + H_1[1 - 2(\sin\phi - \sin\phi_0)^2]. \tag{1e}$$

Here τ is a constant atmospheric relaxation time (commonly set to 2–3 weeks), h_f is the radiative-equilibrium height given by the height scale H_0, half the equator-to-pole height (temperature) difference H_1, and the latitude of maximal forcing (heating) ϕ_0. This form of the radiative-equilibrium height follows the upper branch of the radiative forcing used by Lindzen and Hou (1988).

Equations (1a)–(1e) are nondimensionalized using the following scales: u on Ωa, t on τ, v on a/τ, and h and h_f on H_0. Thus, the natural scale for the angular momentum, $M = \cos\phi a\,(\Omega a\cos\phi + u)$, is Ωa^2. To simplify the subsequent analysis, we make the following substitutions in system (1): M for u, $V = v\cos\phi$ for v, and $\mu = \sin\phi$ for ϕ. Axial symmetry is introduced by setting the longitudinal derivative equal to zero. These substitutions yield the following nondimensional system (where the dot and prime denote derivatives with respect to time and μ, respectively):

$$\begin{aligned}\dot{V} = &-VV' - \frac{\mu}{1-\mu^2}(\alpha_\tau M^2 + V^2) \\ &+ (1-\mu^2)(\alpha_\tau\mu - \alpha_g h')\end{aligned} \tag{2a}$$

$$\dot{M} = -VM', \tag{2b}$$

$$\dot{h} = -(hV)' - (h - h_f), \tag{2c}$$

$$h_f = 1 + h_1(1 - 2(\mu - \mu_0)^2). \tag{2d}$$

Only three nondimensional parameters determine the solutions of this system:

$$\alpha_\tau = (\Omega\tau)^2; \quad \alpha_g = \frac{gH_0\tau^2}{a^2} \quad \text{and} \quad h_1 = \frac{H_1}{H_0}. \tag{2e}$$

Under typical conditions in the planetary troposphere (H_0: 10–12 km, H_1: 1–2 km, and τ: ~20 days), the values of these nondimensional parameters are $\alpha_\tau \sim 10^4$, $\alpha_g \sim 10^4$, and $h_1 \sim 0.2$. Further details of the precise values of these nondimensional parameters used in the present model are provided below in this section.

The representation (2a)–(2c) is simpler than (1a)–(1c) in that the zonal momentum equation in spherical coordinates with rotation (1b) becomes the simple advection equation (2b), no spherical terms exist in the continuity equation (2c), and the regularity of u, v, and h at the poles is assured by the simple boundary condition

$$V(\mu = \pm 1, t) = 0 = M(\mu = \pm 1, t). \tag{2f}$$

In the absence of a source, the conserved quantities of the SWM are the total mass, total angular momentum, and total energy, denoted here as K_h, K_M, and K_ε, respectively. These quantities were derived for the free, two-dimensional shallow-water equations on a sphere by Paldor and Domelevo (2005, personal communication). The total mass (scaled on $4\pi a^2 H_0\rho_0$, where ρ_0 is the mean density of the atmosphere) is

$$K_h = \int_0^h\int_{-1}^1 dh d\mu = \int_{-1}^1 h d\mu, \tag{3a}$$

and Eq. (2c) yields the conservation law for the total mass:

$$\frac{dK_h}{dt} = \int_{-1}^1 Q d\mu. \tag{3b}$$

The total angular momentum is defined by

$$K_M = \int_0^h\int_{-1}^1 M dh d\mu = \int_{-1}^1 Mh d\mu \tag{4a}$$

(and its scale is $4\pi\Omega a^3 H_0\rho_0$). Equations (2c) and (2b) yield the conservation law for the total angular momentum:

$$\frac{dK_M}{dt} = \int_{-1}^{1} QMd\mu. \tag{4b}$$

The total energy of a layer of fluid is the sum of the vertically integrated kinetic and potential energy. The energy per unit height (mass) is

$$\varepsilon = \frac{1}{2}\mathbf{v}\cdot\mathbf{v} + \alpha_g h, \tag{5a}$$

where $\mathbf{v}$ denotes the horizontal velocity vector and, therefore, the total energy is given by

$$K_\varepsilon = \int_0^h \int_{-1}^{1} \varepsilon dh d\mu = \int_{-1}^{1} \left(\frac{1}{2}h\mathbf{v}\cdot\mathbf{v} + \frac{1}{2}\alpha_g h^2\right) d\mu, \tag{5b}$$

scaled on $2\pi a^2 H_0 \rho_0 \, (\Omega^2 a^2(1+1/\alpha_\tau) + \alpha_g H_0)$. Combining Eqs. (2a)–(2c), one obtains the conservation law for the total energy:

$$\frac{dK_\varepsilon}{dt} = \int_{-1}^{1} Q\varepsilon d\mu. \tag{5c}$$

b. Steady states

Steady solutions of Eqs. (2a)–(2c) are obtained by setting the lhs equal to zero. From Eq. (2b) it is clear that a steady state is only possible when either $V = 0$ or $M(\mu) = \text{const}$. Setting $V = 0$ in system (2) yields the *radiative-equilibrium* steady state:

$$V = 0; \quad M^2 = (1-\mu^2)^2[1 + 2R_T(1 - \mu_0/\mu)]; \quad h = h_f, \tag{6a}$$

where $R_T = 2gH_1 / \Omega^2 a^2 = 2h_1\alpha_g / \alpha_\tau$ is the counterpart of HH80's thermal Rossby number and its typical value is ~0.16 (for $H_1 = 1750$ m and $H_0 = 10$ km). The negative root of the angular momentum in Eq. (6b) corresponds to negative and unphysically large zonal velocities and will not be treated here [but, as will be shown in section 3d, the steady attractor sets of (2a)–(2e) are symmetric with respect to the sign of M_0]. The set (6a)–(6c) should be compared with the expressions derived in section 2 of HH80. For equinoctial forcing ($\mu_0 = 0$, the case studied by HH80), the radiative-equilibrium state implies superrotation at the equator ($M > 1$ at $\mu = 0$), which is prohibited by Hide's theorem in a steady viscous atmosphere but does not apply to the Eulerian (inviscid) SWM.

Setting $M = M_0 = \text{const}$ in system (2) yields the *uniform-M* steady state given by

$$V = -\frac{1}{h}\int (h - h_f)d\mu; \quad M = M_0;$$
$$h = h_0 + \frac{h_1}{R_T}\left(\mu^2 - \frac{M_0^2 + \alpha_\tau^{-1}V^2}{1-\mu^2}\right), \tag{7a), (7b), (7c)}$$

where h_0 is the constant of integration of Eq. (2a). It is easily verified that for our choice of h_f Eqs. (6a)–(6c) and (7a)–(7c) can be simultaneously satisfied only at isolated μ points and for special values of the parameters: in general, the form of forcing used here does not permit the radiative-equilibrium and uniform-M states to coexist in any interval of μ.

Since M is real, Eq. (6b) implies that radiative equilibrium can exist only for

$$1 > \frac{B_S}{\mu}, \tag{8a}$$

in which

$$B_S = \frac{2R_T\mu_0}{1 + 2R_T}, \tag{8b}$$

and that radiative equilibrium exists on the equator (i.e., $\mu = 0$) only for $\mu_0 = 0$. For off-equatorial forcing ($\mu_0 \neq 0$) Eq. (8a) does not limit the highest latitude of radiative equilibrium in the winter hemisphere where $\mu\mu_0 < 0$. Note that, although the expressions are similar, Eq. (8) is derived by requiring that M be real whereas the expressions derived by Plumb and Hou (1992) and Emanuel (1995) for radiative-equilibrium steady states are derived as extensions of Hide's theorem (which does not hold in the SWM). More generally, for arbitrary forcing condition (8a) can be written as

$$\frac{h_f'}{\mu} < \frac{\alpha_\tau}{\alpha_g}, \tag{8c}$$

implying that for radiative equilibrium to exist near the equator h_f' has to vanish there. The same conclusion was reached by Lindzen and Hou (1988) and Schneider (2006) for small angle, $\mu \ll 1$ (which is why for off-equatorial heating only uniform-M steady state exists near the equator). It should also be noted that a global uniform-M steady state that satisfies the boundary conditions (2f) only exists for $M_0 = 0$, for which the zonal velocity has an unrealistic value of 1.5 Mach on the equator [i.e., $u(0) = -\Omega a$]. Since in our scaling $V \sim O(1)$, and $\alpha_\tau \sim O(10^4)$, the nonlinear V terms in Eqs. (2a) and (7c) are negligibly small compared to the other terms. This approximation yields explicit expressions for h and V in the global uniform-M steady state, which for $M = 0$ are written as

$$h = 1 + \frac{h_1}{R_T}\left(\mu^2 - 2R_T\mu_0^2 + \frac{R_T - 1}{3}\right) \tag{9a}$$

and

$$V = \frac{(1 + 2R_T + 6R_T\mu_0^2)\mu - 2R_T(\mu - \mu_0)^3 - \mu^3}{R_T(3/h_1 + 1 - 6\mu_0^2) - 1 + 3\mu^2}. \tag{9b}$$

Under this approximation the boundary conditions $V(\mu = \pm 1) = 0$ are exactly satisfied in the equinoctial case, whereas for small $\mu_0 \neq 0$ the error is $O(\mu_0 R_T) \sim 10^{-2}$. It should be noted that both global steady states are unphysical on the equator ($M = 0$ implies unrealistic u while the radiative-equilibrium state implies superrotation), indicating that the physically acceptable steady states of the system consist of combinations of the two steady states.

In both steady states the value of the total mass $\tilde{K}_h$ [which denotes K_h at the steady states according to Eq. (3a)] is given by

$$\tilde{K}_h = \int_{-1}^{1} h_f d\mu = 2\left[1 + h_1\left(\frac{1}{3} - 2\mu_0^2\right)\right]. \qquad (10)$$

Equations (6a)–(6c) and (7a)–(7c) indicate that the steady solutions of Eqs. (2a)–(2c) depend on R_T and μ_0 [i.e., a particular combination of the model parameters in Eq. (2e)]. In the present study we only consider the $\mu_0 = 0$ case: the effect of off-equatorial heating is left for a sequel study. Effectively, R_T is a Richardson number that quantifies the available potential energy (scaled on the square of the velocity scale). In the present shallow-water model, in which the height is proportional to temperature, the value of H_0 is arbitrary (provided only that $H_1 < H_0) \ll \alpha$ as it affects only the expression for h in the uniform-M steady state. The ambiguous interpretation of the height as both geopotential height and temperature is settled in this work by the choice of the values of H_0 and H_1 such that h_1 ($= H_1/H_0$) models the ratio between the equator to pole temperature difference and the mean tropospheric temperature, whereas H_1 models the equator to pole geopotential difference. In addition, the tropical circulation on earth is characterized by a strong shear between its upper branch, dominated by poleward angular momentum–conserving flow, and its drag-dominated lower branch. In the inviscid limit—the nature of the viscosity (i.e., turbulent or molecular) is not relevant in this case—the circulation becomes predominantly barotropic, following the upper angular momentum–conserving branch of the circulation with a thin bottom boundary layer (Williams 2003). Therefore, although the effective thickness of the upper—presumably isentropic—branch of the Hadley circulation on earth is relatively thin [~400 m in the tropics for a linear model where the shape of the tropopause is externally enforced, Held and Phillips (1990)], the SWM applies to an inviscid layer whose geopotential height is essentially the height of the bulk of the tropopause.

3. Analytical and numerical solutions for $\mu_0 = 0$

a. The relationship between initial conditions and steady states

A simple choice of initial conditions, commonly used in previous studies, is a motionless atmosphere with uniform height; that is,

$$\begin{aligned} u(\mu, 0) &= 0 \Leftrightarrow M(\mu, 0) = 1 - \mu^2, \\ V(\mu, 0) &= 0, \\ h(\mu, 0) &= \text{const}, \end{aligned} \qquad (11a), (11b), (11c)$$

which guarantees that h and M are symmetric and V is antisymmetric with respect to μ. The relevance of these symmetric initial conditions to more general ones is bolstered by our finding (numerical results, not shown) that for mixed, symmetric and antisymmetric initial conditions the inherent symmetry of h_f imposes its symmetry on $h(\mu)$, causing $V(\mu)$ to be antisymmetric and $M(\mu)$ to be symmetric after sufficiently long times. For a symmetric $M(\mu)$ and an antisymmetric $V(\mu)$ Eq. (2b) implies:

$$\begin{aligned} \left.\frac{\partial M}{\partial t}\right|_{\text{equator}} &= 0, \\ V(0, t) &= 0, \\ M(0, t) &= M_0(= \text{const}), \end{aligned} \qquad (12a), (12b), (12c)$$

indicating that the asymptotic state of the system depends critically on $M(\mu, t = 0)$. Note that hemispherical symmetry is imposed on the forcing but not on the solutions; that is, the vanishing of the meridional flux at the equator is not a boundary condition (as is the case in HH80). In our numerical integrations the above inferred symmetry of $M(\mu)$ and asymmetry $V(\mu)$ is realized for both symmetric (at short times) and antisymmetric (after long times) initial conditions. It follows from Eqs. (6a)–(6c) and (7a)–(7c) that for the radiative equilibrium to be reached at the equator M has to be initiated with $M(\mu = 0) = \sqrt{1 + 2R_T}$ while the uniform-M state can be reached there only if $M(\mu = 0) = 0$ initially. Indeed, when integrations were initiated with $V(\mu)$ and $h(\mu)$ near those of Eqs. (3a)–(3c) and (4a)–(4c) but with the above values of $M(\mu = 0)$, the steady states reached by the system after long times were, as expected, the global radiative-equilibrium and uniform-M states, respectively.

b. Numerical scheme

Time integrations of system (2) were performed using a staggered grid (where h is staggered from V and M) leapfrog scheme with a Robert–Asselin time filter ($\alpha = 0.001$). It is well known that, as diffusion tends to zero,

smooth solutions of the shallow-water equations converge to discontinuous (weak) solutions. As implied by HH80 and shown in the next section, this is the case with Eq. (2b). As solutions of Eq. (2b) approach a jump, two problems arise with the aforementioned leapfrog scheme [which is centered in time and space in the case of Eq. (2b)]. First, previous analysis of the linearized shallow-water equations has shown that, while damping the computational mode inherent in the leapfrog scheme, the Robert–Asselin filter may also significantly damp the physical mode and introduce a phase error as well as instabilities (Schlesinger et al. 1983; Déqué and Cariolle 1986). The damping and phase error of the physical mode strengthen with the frequency of the mode. Therefore, as a jump is approached, the Robert–Asselin time filter is expected to halt the formation of the jump by damping the highest frequency mode and introduce phase errors. Secondly, the leading term in the truncation error of the space-centered scheme used to integrate Eq. (2b) contains a dispersive third-order derivative. As the jump is approached, the effect of dispersion is to introduce high amplitude oscillations near the jump, as can be seen in Fig. 2c, where such oscillations just begin to form). This effect is suppressed by maintaining the dispersion (proportional to Δx^2) negligible compared to the diffusion (LeFloch 2002). The first problem is delayed and the second is remedied by increasing the spatial resolution and choosing the lowest temporal resolution for which the scheme is stable. The temporal resolution used in the integrations presented in the next sections is 10^{-5} and the spatial resolution is 1/450 in μ, which translates to a resolution of 0.25° at the equator, about 0.4° at midlatitudes, and 7.6° at the poles.

Although viscosity is not explicit in the SWM, numerical viscosity is implicitly introduced in any numerical scheme, and it is worth considering its effect on the solution. Toward this end we have integrated the time-dependent system with a second-order viscous term added to Eqs. (2a) and (2b) while keeping the temporal and spatial resolution unchanged. We found that the states reached from the same initial conditions were identical for viscosity coefficients ranging between 10^{-10} and 10^{-20}. This comparison indicates that the results presented in the next section are qualitatively unaffected by the inclusion of numerical viscosity and the Eulerian limit of the solutions of Eq. (2b) is approached by our numerical scheme. The value of the viscosity coefficient used in the integrations presented in the next sections is 10^{-15}.

c. Numerical solutions of the initial value problem

Time integrations indicate that for $0 < M_0 < \sqrt{1 + 2R_T}$ the equinoctial asymptotic long-time behavior is characterized by a tropical uniform-M region and an extratropical radiative-equilibrium region and that these two regions are connected by an unsteady transition region whose width, $\Delta\mu$, decreases monotonically with time. In the $\Delta\mu \to 0$ limit the transition region becomes a transition point, referred to as $\mu_J = \sin\phi_J$, at which M is discontinuous but V and h are continuous. This limit, however, is not realized even after times $O(10^3)$, that is, dimensional time $O(10$ yr). Hereafter we shall refer to this limit as the (steady) attractor set $[V_A(\mu), M_A(\mu), h_A(\mu)]$ defined as stable steady states of the equations that are reached by phase space trajectories after long times.

Equation (2b) is an advection equation for which the existence of smooth solutions at all times $t > 0$ is not guaranteed (cf. Evans 1998). The vanishing of V near μ_J drastically slows down the temporal change in M in the transition region, causing the discontinuity (or shock) in M there to be reached only after very long times. For the reasons described in section 3b, it is not possible to determine the time it takes the shock to form using the numerical scheme used in this work. It is clear, however, that the time it takes the shock to form far exceeds the duration of a season, allowing us to set it at infinity without affecting the physical generality and interpretation of our results. In agreement with our previous analysis, the existence of an ever-narrowing unsteady transition region suggests that (with the exception of the two special cases mentioned in section 2b) steady states are not reached even at long (but finite) times. The state of the system at sufficiently long times is therefore more precisely described as a *near-steady state* (NSS). Let $\mu_T(t)$ and $\Delta\mu(t)$ be the location of the equatorward boundary of the transition region and the width of this region, respectively, at time t. The NSS is then defined by

$$\begin{cases} \dfrac{\partial}{\partial t}(V(\mu,t), M(\mu,t), h(\mu,t)) = 0 & \text{for} \quad |\mu| < |\mu_T(t)| \quad \text{and} \quad |\mu| > |\mu_T(t) + \Delta\mu(t)| \\ \dfrac{\partial}{\partial t}(V(\mu,t), M(\mu,t), h(\mu,t)) \neq 0 & \text{for} \quad |\mu_T(t)| < |\mu| < |\mu_T(t) + \Delta\mu(t)|. \end{cases} \tag{13}$$

A schematic illustration of the NSS is given in Fig. 1, where the uniform-M and radiative-equilibrium steady states prevail near the equator (Region I) and near the poles (Region III), respectively, whereas no steady state

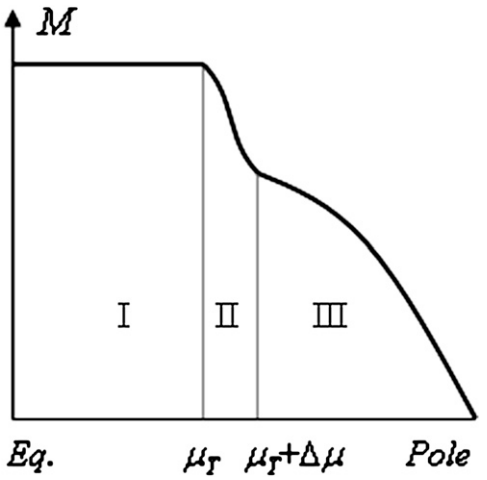

FIG. 1. Sketch of the meridional profile of M in the three regions of the equinoctial NSS; μ_T and $\Delta\mu$ denote the equatorward boundary of the transition region and its width, respectively. The designation of the regions follows the distribution of M: I is steady uniform-M [$M(t) = M_0$], II is unsteady transition region [$M(t)$ connects M_0 with max($M_{\rm RE}$) across the transition region], and III is steady radiative equilibrium [$M(t)=M_{\rm RE} = (1-\mu^2)(1+2R_T)^{1/2}$].

is reached in the narrowing transition region between them (Region II). The asymptotic limit of $\mu_T(t\to\infty)$ (and $\Delta\mu\to 0$) is μ_J. Figure 2 displays snapshots (t =20, 200, and 500) of the evolution of the equinoctial NSS when the system is initiated by

$$M(\mu,0) = (1+U_0)(1-\mu^2),$$
$$V(\mu,0) = 0,$$

and

$$h(\mu,0) = \frac{1}{2}\tilde{K}_h, \qquad (14a)(14b),(14c)$$

with $\tilde{K}_h$ given by Eq. (10) and $U_0 = -0.1$. The three panels in Fig. 3 display the state of the system at $t = 500$ when the system is initiated with $U_0 = 0$, 0.1, and 0.2 in Eq. (14). The analytically obtained solution (see section 3d) for the angular momentum in the attractor set $M_{\rm A}(\mu)$ [given by Eq. (7b) for $|\mu| < \mu_J$ and by Eq. (6b) for $|\mu| > \mu_J$] is also shown for reference. The total mass, angular momentum, and energy as a function of time, corresponding to $0 \le t \le 100$ for the integration of Fig. 2, are shown in Fig. 4. The meridional distribution of the volume flux Vh, momentum flux VM, and zonal velocity flux Vu corresponding to Fig. 2b and the states of the system corresponding to Fig. 3 at $t = 200$ are shown in Fig. 5, which should be compared to Fig. 1 in Walker and Schneider (2005) and Fig. 7 in HH80. Our scaling of V on a/τ ensures that at sufficiently long times the nondimensional amplitude of all fluxes is independent of the value of τ and that the three fluxes have the same scale (cf. Fang and Tung 1997).

The transient behavior that develops when system (2) is initialized away from the attractor set is characterized by a strong meridional wind and fast gravity wave oscillations that diminish within about $t = 20$. The uniform-M and radiative-equilibrium regions grow from the respective boundaries toward their asymptotic transition point μ_J. The reduced meridional fluxes at the transition region cause the system to evolve very slowly there, as seen in Fig. 2, where even at $t = 200$ the width of the transition region is still about 10°.

A measure of the narrowing of the transition region width $\Delta\phi(t)$ [the counterpart of $\Delta\mu(t)$ in degrees latitude] is plotted in Fig. 6a, where $\phi_J - \phi_T(t)$ [which corresponds to $\mu_J - \mu_T(t)$] is plotted versus time for two combinations of M_0 and R_T, both of which yield $\mu_J = 0.5$ (30°): $M_0 = 1$, $R_T = 0.204$ (solid) and $M_0 = 0.9$, $R_T = 0.0704$ (dashed). Degrees of latitude are used instead of μ for clarity. The equatorward boundary of the transition region, $\phi_T(t)$, is defined as the most equatorward point for which $M(\phi) < M_0$. To avoid any ambiguity associated with the oscillating poleward boundary of the transition region, the evolution of $\phi_J - \phi_T(t)$ is used as a measure of half the transition region width as $t \to \infty$ instead of $\Delta\phi(t)$. In Fig. 6b the amplitude of the corresponding $V(\phi, t = 500)$ is plotted versus latitude for the two cases. It is evident that the rate of the narrowing of the transition region [indicated by the rate of increase of $\phi_T(t)$] follows the local amplitude of V, which is maximal/minimal near the point in the tropics where $h = h_f$ and vanishes close to the transition point. Identical results to those shown in Fig. 6 were reproduced with numerical viscosity coefficients in the range of 10^{-10}–10^{-20} and with a Robert–Asselin time filter coefficient in the range of 10^{-3}–10^{-4}, indicating that for $t < 500$ the solutions have not been affected by our choice of numerical parameters.

The subtropical jet (defined as the latitude of maximal u) seen in Figs. 2 and 3 is located within the boundaries of the transition region; that is, it forms poleward of, and slowly shifts toward, $\mu_T(t)$ while strengthening [and while $\mu_T(t)$ itself slowly moves toward μ_J]. Note that the (rather slow) rate at which M coalesces toward a jump at μ_J is a property of the inviscid, time-dependent, equations: similar results were encountered with a wide range of numerical viscosity coefficients explicitly introduced into the numerical scheme, as explained in section 3b.

For $M_0 > \sqrt{1+2R_T}$, the uniform-M region is reduced to a point on the equator (i.e., $\mu_J = 0$; see Figs. 3c and 7). The tropical cell disappears altogether in this case and a single westerly equatorial jet forms while

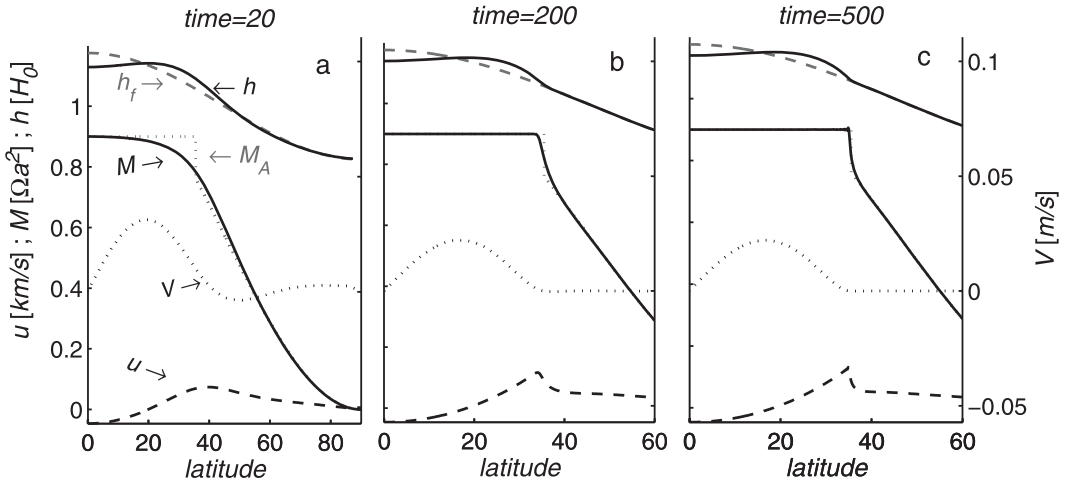

FIG. 2. Near-steady states at t = (a) 20, (b) 200, and (c) 500 initiated with $M_0 = 0.9$, $\alpha_g = 18\tau^2$, $\alpha_\tau = (2\pi\tau)^2$, and $h_1 = 0.175$ ($R_T = 0.16$; $\tau = 20$ days). The shapes of M in the attractor set, M_A, and of h_f are shown for reference in gray. The dimensional scales for the two heights, h (upper solid) and h_f (upper dashed gray); for the two angular momenta, M (middle solid) and M_A (dotted gray); and the zonal velocity u (lower dashed) are given on the left ordinate of (a) and the dimensional scale of V (lower, dotted) is given on the right ordinate of (c). The formation of the NSS that consists of a tropical ($\mu < \mu_T$) uniform-M region—an unsteady transition region ($\mu_T < \mu < \mu_T + \Delta\mu$) connecting the tropical region with the extratropical ($\mu_T + \Delta\mu < \mu$) radiative-equilibrium region—is clearly evident in the profile of M. In (b) and (c) the meridional range in the abscissa is truncated at 60° since poleward of it radiative equilibrium is fully established at $t > 20$. The values of (μ_T, $\Delta\mu$) in (a), (b), and (c) correspond to (ϕ_T, $\Delta\phi$) of (3.5°, 50°), (30°, 10°) and (35°, 5°), respectively. For comparison with the analytical estimate, the value of μ_J from Eq. (16a) is 0.581 (i.e., ϕ_J =35.52°).

upgradient fluxes develop near the equator in the, now tropical, transition region.

d. Analytical solutions for the attractor set

As discussed in section 2b, we may neglect the nonlinear V terms in Eqs. (2a) and (7c) for $\tau > 1$ (this is also a required condition for the self-consistency of the nearly-inviscid theory; see HH80). Under this approximation, Eq. (2a) yields a spherical–geostrophic balance between $h'(\mu,t)$ and $M(\mu,t)$ at all times (analogous to the cyclostrophic balance discussed in Fang and Tung 1996). At steady state, this implies that the only parameters of the problem are R_T ($\propto \alpha_g/\alpha_\tau$) and M_0, so μ_J is independent of τ. To determine μ_J we assume continuity of h (which plays the role of density) at μ_J and require mass conservation; that is,

$$\int_0^{\mu_J} (h - h_f)d\mu = 0. \tag{15}$$

Carrying out the integration, one obtains the relation $\mu_J(M_0, R_T)$ by the roots of the transcendental equation:

$$B_E\left[\frac{\mu_J}{1-\mu_J^2} - \frac{1}{2}\ln\left(\frac{1+\mu_J}{1-\mu_J}\right)\right] = \frac{2}{3}\mu_J{}^3, \tag{16a}$$

where

$$B_E = \frac{M_0^2}{1+2R_T}. \tag{16b}$$

The attractor sets are given by Eqs. (6a)–(6c) poleward of μ_J and by Eqs. (7a)–(7c) equatorward of μ_J. Figure 7a gives the complete solution for μ_J as a function of B_E following Eq. (16a). Solutions for $B_E > 0.44$ are shown explicitly in Fig. 7b as contours of M_0 on the (R_T, μ_J) plane. The $M_0 = 1$ contour is identical to the solutions of Eq. (17) of HH80. The $M_0 > 1$ contours in Fig. 7b and the $M_0 > 1$ cases in Figs. 3 and 5 represent superrotating states, which are prohibited by Hide's theorem, so they do not represent vertically diffusive steady states. Nonetheless, these states are presented here for the completeness of the SWM's analysis.

Although the analytic estimate for μ_J in Eq. (16a) is obtained by requiring $\tau > 1$, numerical integrations of the time-dependent equations have demonstrated that solutions of Eq. (16a) were shifted poleward by less than 2° in the limit $\tau \ll 1$, in agreement with the results of Fang and Tung (1997).

Our numerical integrations indicate that initial conditions in which $M(\mu,0)$ does not decrease monotonically from the equator to the poles introduce instabilities that can be overcome only by employing significantly larger numerical viscosities. We therefore restrict the collection of all initial conditions giving

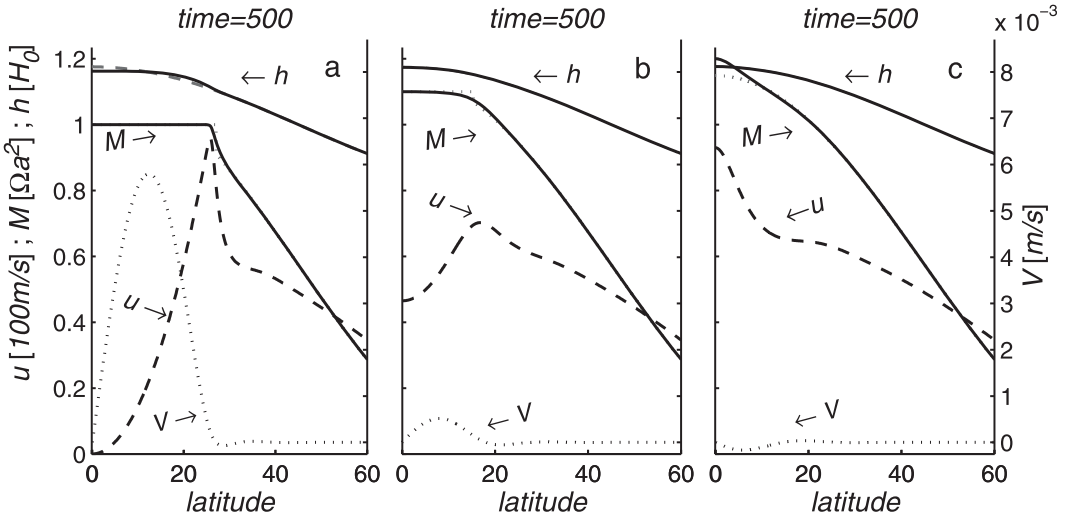

FIG. 3. As in Fig. 2c ($t = 500$) but the scale of u is 100 m s^{-1}: (a) $U_0 = 0$ ($M_0 = 1.0$) with values of μ_T, $\Delta\mu$, and μ_J (given by Eq. 16a) of 0.4, 0.21 and 0.456, respectively (i.e., ϕ_T, $\Delta\phi$, and ϕ_J of 24°, 14°, and 27.11°, respectively); (b) $U_0 = 0.1$ ($M_0 = 1.1$) with values of μ_T, $\Delta\mu$, and μ_J of 0.04, 0.36, and 0.265, respectively (i.e., ϕ_T, $\Delta\phi$, and ϕ_J of of 2°, 21°, and 15.35°, respectively); (c) $U_0 = 0.2$ ($M_0 = 1.2$) with values of μ_T, $\Delta\mu$, and μ_J of 0, 0.32 (i.e., $\Delta\phi \approx 19°$), and 0, respectively. Note that the scale on the ordinate for V is three orders of magnitude smaller than in Fig. 2.

rise to trajectories that approach a certain attractor set (hereafter referred to as the basin of attraction of that attractor set) to monotonically decreasing profiles of M between the equator and the poles. This restriction on $M(\mu,0)$ is consistent with an extrapolation of Hide's theorem [which mandates $\mu M' \le 0$ everywhere; see Plumb and Hou 1992; Emanuel 1995)] to the SWM.

The values of the total mass, angular momentum, and energy of the attractor set, denoted $(K_h^A, K_M^A, K_\varepsilon^A)$, can be calculated by specifying μ_J. Using Eq. (16a) for μ_J and neglecting the quadratic V terms, the total angular momentum is given by

$$K_M^A = 2\int_0^{\mu_J} M_0 h_f \, d\mu + 2\int_{\mu_J}^{1} \sqrt{1+2R_T}(1-\mu^2)h_f \, d\mu \qquad (17)$$

and the total energy by

$$K_\varepsilon^A = \int_0^{\mu_J} \left[\alpha_\tau h(\mu)\left(\frac{M_0^2}{1-\mu^2} + 1 - \mu^2 - 2M_0\right) + \alpha_g h(\mu)^2\right] d\mu + \int_{\mu_J}^{1} \{\alpha_\tau h_f [2(1-\mu^2) \times (1 + R_T - \sqrt{1+2R_T})] + \alpha_g h_f^2\} d\mu, \qquad (18)$$

where $h(\mu)$ is given by Eq. (7b). The explicit algebraic expressions obtained by carrying out the integrations in Eqs. (17) and (18) are too complex and unrevealing to be presented here. We also note that $\tilde{K}_h$ is the total mass in the attractor set; that is, $K_h^A = \tilde{K}_h$; see Eq. (10).

The total tropical mass flux, often referred to as the strength of the tropical circulation and denoted here as

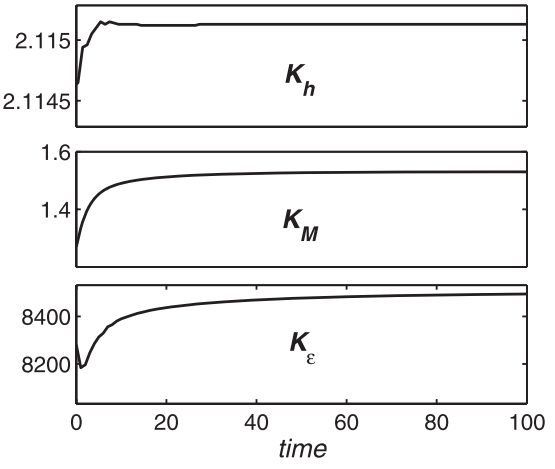

FIG. 4. Angular momentum, K_h, K_M, and K_ε, for $0 \le t \le 100$, corresponding to the time series displayed in Fig. 2. Mass (h) is conserved after $t \approx 20$ with the predicted value for $\tilde{K}_h$; K_M is nearly conserved after $t \approx 50$ while the increase in K_ε, which is coupled to the strengthening of the subtropical jet, continues slowly to $t \to \infty$ where it asymptotes to the value given by the integrals in Eq. (18).

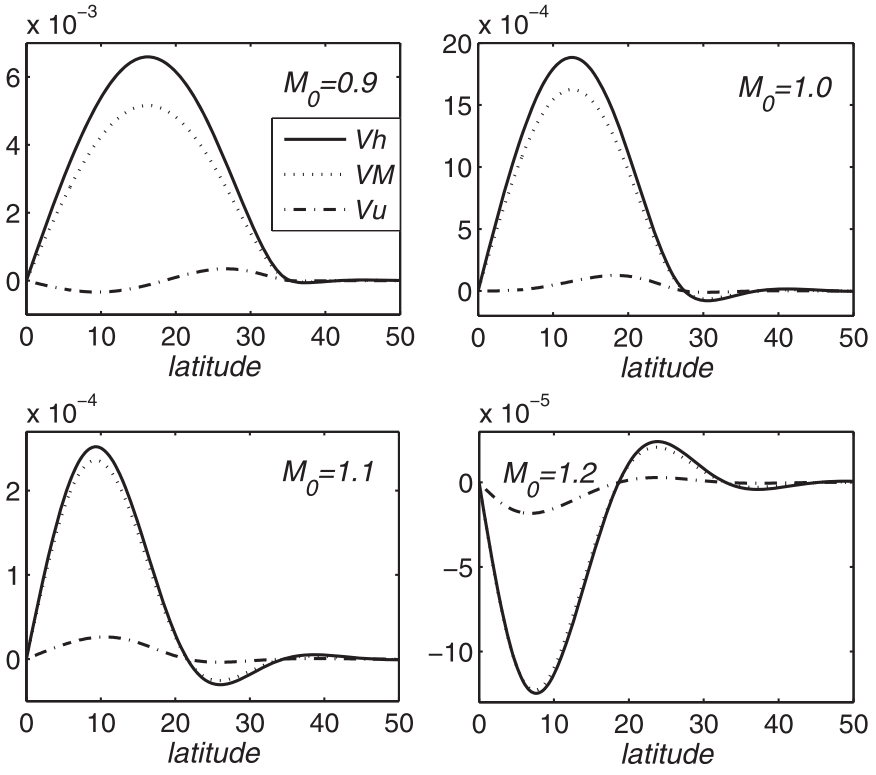

FIG. 5. Meridional distribution of the (nondimensional) meridional fluxes corresponding to the states of the system displayed in Figs. 2 and 3 at $t = 200$ for the indicated values of M_0. Solid lines: volume flux (Vh, related to the mass flux via the mean density of the atmosphere) scaled on $2\pi aH_0/\tau$; dotted lines: angular momentum flux (VM) scaled on $2\pi\Omega a^3/\tau$; dashed lines: zonal velocity flux (Vu) scaled on $2\pi\Omega a^2/\tau$.

K_{Vh}, is explicitly calculated by neglecting the quadratic V terms in Eq. (7c), which yields

$$K_{Vh}^A = \int_0^{\mu_J} Vh d\mu = \frac{h_1(1+2R_T)}{2R_T} \times \left[B_E \left(\ln(1-\mu_J^2) + \frac{\mu_J^2}{1-\mu_J^2} \right) - \frac{\mu_J^4}{2} \right]. \quad (19)$$

The value of K_{Vh} is determined by h_1, R_T, and B_E; Figs. 8a and 8b show the solutions for K_{Vh} in Eq. (19) when B_E and h_1 are varied, respectively.

Using Eqs. (16a) and (16b) and Eq. (6b) it can be easily verified that M decreases monotonically with μ in the attractor set and that

$$\max[(1-\mu^2)\sqrt{1+2R_T}] < M_0. \quad (20)$$

Since the lhs of (20) is the maximum angular momentum in the radiative-equilibrium steady state, the strong inequality implies that no attractor set exists for which the radiative-equilibrium and uniform-M states are continuously connected; that is, in equinoctial forcing no steady states of system (2) exist other than the two states given in section 2b.

It is possible to obtain explicit near-steady solutions for V, M, and h for $\Delta\mu > 0$ by specifying the shape of M in the transition region and requiring the continuity of M and h and mass conservation. Solutions obtained using linear and quadratic approximations for M in the transition region (not shown) were found to be in agreement with the numerical time integrations once the size of the transition region has shrunk to less than 15°.

It follows from Eq. (16a) that μ_J depends strongly and nonlinearly on M_0 and R_T. Thus, with reference to the results of Figs. 2 and 3 and employing the estimates for the amplitudes of the subtropical and equatorial jets,

$$u_J = \frac{M_0}{\cos\phi_J} - \cos\phi_J$$

and

$$u_{\text{eq}} = M_0 - 1, \quad (21a), (21b)$$

one can draw the following conclusions regarding axisymmetric variations (for a fixed value of R_T): When M_0 is slightly less than 1 (Fig. 2), the tropical cell will widen and strengthen, the subtropical jet will strengthen [Eq.

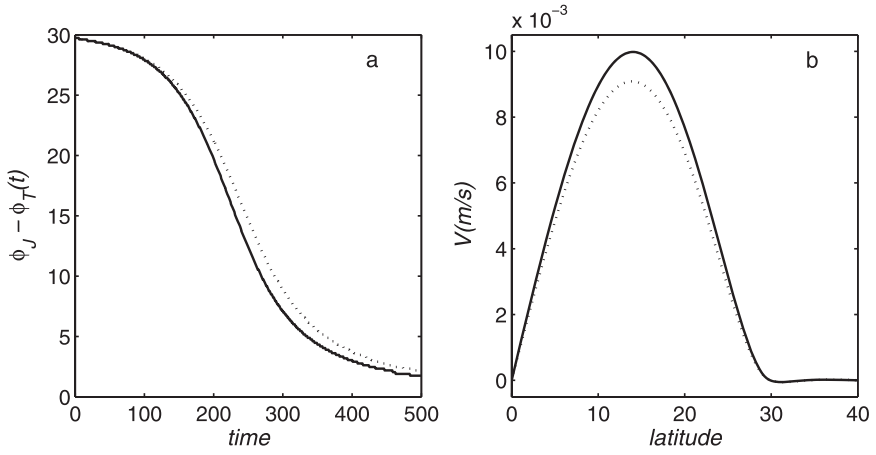

FIG. 6. (a) A measure of half the transition region's width, $\phi_J - \phi_T(t)$, as a function of time for two combinations of M_0 and R_T, both of which yield $\mu_J = 0.5$ (i.e., $\phi_J = 30°$): $M_0 = 1$ and $R_T = 0.204$ (solid); $M_0 = 0.9$ and $R_T = 0.0704$ (dotted). (b) The meridional structure of the amplitude of the corresponding meridional velocities at $t = 500$. At earlier times the meridional structures are similar.

(21a) with $M_0 \leq 1$, but ϕ_J given by Eq. (16a)] and shift to higher latitudes (μ_J increases), and equatorial easterlies will form (21b). In contrast, for M_0 slightly above 1 (but less than $\sqrt{1 + 2R_T}$: Fig. 3b) one can expect the tropical cell to narrow and weaken, the subtropical jet to weaken and shift to lower latitudes, and equatorial westerlies to form. When $M_0 > \sqrt{1 + 2R_T}$ ($B_E > 1$: Fig. 3c) the size of the tropical cell is reduced to zero, making $\mu_J = 0$ so that the subtropical jet becomes a point of discontinuity on the equator coalescing with the equatorial westerly.

Similarly, for a fixed value of M_0 we deduce from Fig. 7b that, when R_T is slightly increased, the tropical cell widens but its strength varies according to Eq. (19) and the subtropical jet strengthens [Eq. (21a) with M_0 fixed, but ϕ_J given by Eq. (16a)] and shifts to higher latitudes with no effect on the equatorial easterlies. In contrast, when R_T is slightly decreased one can expect the tropical cell to narrow and the subtropical jet to weaken and appear at lower latitudes.

Under physically plausible conditions, changes in the atmosphere are likely to be the result of variations in h_1.

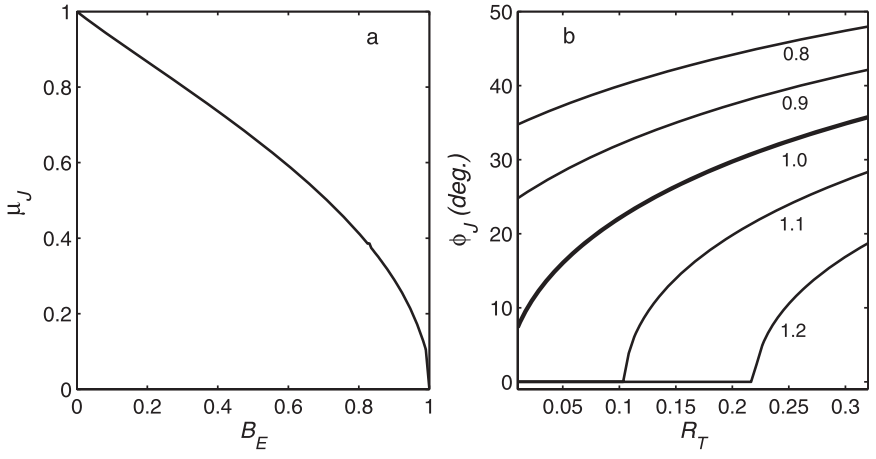

FIG. 7. (a) Solutions of Eq. (16a) for μ_J as a function of B_E in the range $0 < B_E \leq 1$ [$B_E = M_0^2/(1 + 2R_T)$]; $B_E = 1$ corresponds to the global uniform-M state and $B_E = 0$ corresponds to the global radiative-equilibrium state. For $B_E > 1$ the only solution is the trivial solution $\mu_J = 0$, which exists for all values of B_E. (b) Contours of M_0 on the (R_T, ϕ_J) plane. The emphasized $M_0 = 1$ contour is identical to the solutions of Eq. (17) of HH80. The parameters μ_J, M_0, and R_T completely determine the steady attractor set made up of Eqs. (6a)–(6c) poleward of μ_J and Eqs. (7a)–(7c) equatorward. Note that $B_E > 0.44$ in the ranges of M_0 and R_T shown in (b).

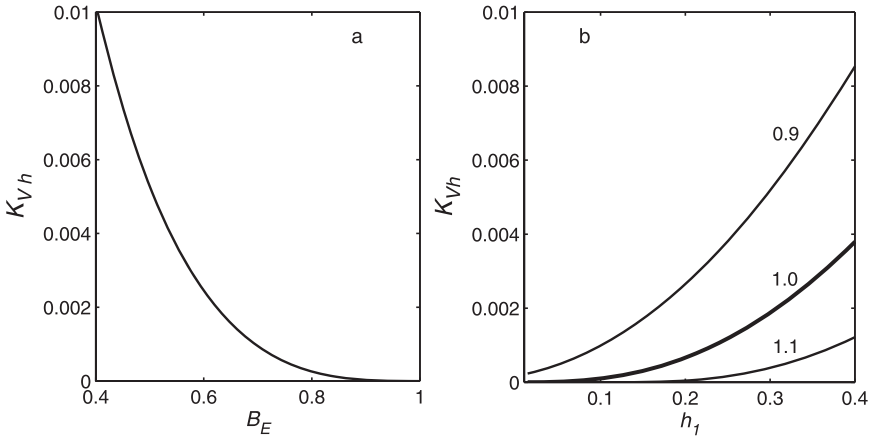

FIG. 8. (a) Solutions of Eq. (19) for K_{Vh} as a function of B_E in the range $0.4 < B_E \leq 1$ [where $B_E = M_0^2/(1 + 2R_T)$]. The value of h_1 is fixed to 0.175. (b) Contours of M_0 on the (K_{Vh}, h_1) plane for $0.01 < h_1 < 0.4$. The $M_0 = 1$ contour is emphasized.

Thus, from Fig. 8 we may conclude that an increase in the equator-to-pole height difference (i.e., an increase in H_1) or a mean cooling of the atmosphere (i.e., a decrease in H_0) will result in an increase in the axisymmetric circulation strength and vice versa.

4. Physical considerations of the mass/heat source

A compressible column of air can be heated without altering its momentum (and vice versa). The coupling of the temperature and total mass of a column of air by its height in the incompressible SWM implies that the local supply of heat takes place by adding mass with the same local momentum as the fluid. Conversely, a local supply of mass is coupled to an increase in the temperature of the column. To resolve some of this ambivalence in the nature and interpretation of the forcing (i.e., whether it is heat or mass) we examine in this section the nature of the source term in Eq. (2c) by considering two modifications to the SWM: a stationary bottom layer as a mass source and a total angular-momentum-conserving model. The former emphasizes the role of the source as a mass source and the latter compensates for momentum added to or removed from the system by mass, thereby making the source a pure heat source. In addition, the contribution of moist convective sources in the SWM is considered in section 4c.

Other possible sources that can significantly influence the zonal mean flow at the tropics such as the earth's obliquity (which acts as a negative momentum source) and transient eddies [which act as a positive momentum source, Lee(1999)] are not treated here.

a. Stationary bottom layer as a mass source

If one assumes that the source of mass is a stationary bottom layer that does not interact with the upper isentropic layer except for the exchange of mass, the zero relative momentum of the air supplied by the bottom layer introduces a momentum forcing in Eqs. (2a) and (2b) of the form (Esler et al. 2000; Shell and Held 2004)

$$I\frac{Q}{h}\begin{pmatrix} V \\ M - 1 + \mu^2 \end{pmatrix}, \quad \text{where} \quad I = \begin{cases} -1, & Q > 0 \\ 0, & Q \leq 0. \end{cases} \tag{22}$$

[The upper/lower rows are the source terms for Eqs. (2a) and (2b), respectively.] For $I = -1$ this forcing introduces an additional steady state in which h is not in radiative equilibrium and M is not uniform. Consequently, in contrast to the results presented in section 3, the resulting axisymmetric 1½-layer model (hereafter referred to as a 1½-SWM) depends very weakly on the choice of initial conditions. With the addition of the forcing terms of Eq. (22), system (2) reaches a global radiative-equilibrium steady state after long times when initiated from a perturbation of (i.e., near) the state (3a)–(3c). All other physically acceptable initial conditions yield a steady state in which $M = 1$ (i.e., $u = 0$) at the equator (this result can be generalized to $M = 1 + u_0$ for a nonstationary bottom layer with velocity u_0). This is explained by the symmetry of the system that mandates $VM' = 0$ at the equator so that, when the forcing is modified according to Eq. (22), either $M = 1$ or $h = h_f$ must be satisfied.

Thus, the steady state of the 1½-SWM entails a three-region paradigm: a tropical, mass-acquiring region; a subtropical, mass-depleting, uniform-M region; and an extratropical radiative-equilibrium region. Shell and Held (2004) approximate this state using small μ approximations of the $M \approx 1$ solutions of Eq. (16a). If we assume instead that the uniform-M state exists poleward of the latitude, $0 < \bar{\mu} < \bar{\mu}_J$ (where $\bar{\mu}_J$ denotes the

location of the subtropical jet in the 1½-SWM), and that the value of M in this region is close to 1, then the continuity of h implies that

$$(1 + 2R_T)(1 - \bar{\mu}_J^2)(1 - \bar{\mu}^2) = 1. \tag{23}$$

If we also require $\bar{\mu} \ll 1$, we obtain the approximation

$$\bar{\mu}_J \simeq \tilde{\mu}_J = \sqrt{2R_T/(1 + 2R_T)}. \tag{24}$$

A more accurate approximate solution is obtained by requiring that h be uniform in the mass-acquiring region. The state of the system is then approximated by

$$\begin{aligned} M &= 1 - \frac{\bar{\mu}^2\mu^3 - \frac{3}{5}\mu^5}{3\bar{\mu}^2\mu - \mu^3}, \\ h &= \bar{h} = \text{const}, \\ V &= \frac{2h_1}{\bar{h}}\left(\bar{\mu}^2\mu - \frac{1}{3}\mu^3\right) \end{aligned} \tag{25}$$

in the mass acquiring region, by Eqs. (7a)–(7c) in the mass depleting region, and by Eqs. (6a)–(6c) in the extratropical radiative-equilibrium region. Solutions of this state are obtained by requiring the continuity of h at both $\bar{\mu}$ and $\bar{\mu}_J$, which yields

$$B_E = (1 - \bar{\mu}_J^2)(1 - \bar{\mu}^2), \tag{26a}$$

where, from Eq. (25), $M_0 = 1 - \frac{1}{5}\bar{\mu}^2$, the continuity of M at $\bar{\mu}$ and the conservation of mass implies that

$$\begin{aligned} B_E\left[\frac{\bar{\mu}_J - \bar{\mu}}{1 - \bar{\mu}_J^2} - \frac{1}{2}\ln\left(\frac{(1 + \bar{\mu}_J)(1 - \bar{\mu})}{(1 - \bar{\mu}_J)(1 + \bar{\mu})}\right)\right] \\ = \frac{\bar{\mu}^3}{3}\left(\frac{1 + 6R_T}{1 + 2R_T}\right) + \frac{2\bar{\mu}_J^3}{3} - \bar{\mu}_J^2\bar{\mu}. \end{aligned} \tag{26b}$$

Solutions of Eqs. (26a) and (26b) for $\bar{\mu}_J(\bar{\phi}_J)$, $\bar{\mu}(\bar{\phi})$, and $\tilde{\mu}_J(\tilde{\phi}_J)$ are compared in Fig. 9a with the corresponding SWM value of ϕ_J given by the $M_0 = 1$ contour of Fig. 7b. The solution of the time-dependent equations (at t = 500) of the 1½-SWM initiated by the initial conditions [(11a)–(11c)] is compared with the state approximated by Eqs. (26a) and (26b) in Fig. 9b for $R_T = 0.16$. The steady solutions of the 1½-SWM differ from those of the SWM by the existence of a tropical mass acquiring region that connects continuously to the subtropical, mass depleting, uniform-M region. The three-region paradigm of the 1½-SWM appears to be in better agreement with the numerical results of HH80 (their Fig. 6 for the lowest viscosity case) than the two-region paradigm of the one-layer model. As pointed out by HH80, a uniform-M region exists poleward of a tropical region in which vertical mixing of momentum is significant (the rising branch of the Hadley cell). The monotonic decrease of M between the equator and poles and the discontinuity in M at the transition between the uniform-M and the radiative-equilibrium regions is also retained in the 1½-SWM. The monotonic decrease of M mandates that its value in the uniform-M region be slightly less than 1, which accounts for the poleward shift in the location of the subtropical jet compared to the $M_0 = 1$ solution of the 1-layer model (the shift is also captured by $\tilde{\phi}_J$, as shown in Fig. 9a).

b. Conservation of total angular momentum

The conservation of total angular momentum K_M in the presence of a source of mass is achieved by introducing a momentum forcing in Eqs. (2a) and (2b) of the form

$$-\frac{Q}{h}\begin{pmatrix} V \\ M \end{pmatrix}. \tag{27}$$

At steady state this addition introduces the constraint

$$VMh = 0. \tag{28}$$

Consequently, since K_M is conserved, the steady states of the total angular momentum–conserving model have to be either global $V = 0$, corresponding to $\hat{K}_M = 4\sqrt{1 + 2R_T}\left(\frac{1}{3} + \frac{1}{5}h_1\right)$ or $M = 0$ (i.e., $K_M = 0$). Combinations of the two states are also possible and these consist of a tropical $M = 0$ region that is discontinuously connected to an extratropical radiative-equilibrium region for $0 < K_M < \hat{K}_M$. No steady state exists for $K_M > \hat{K}_M$ (in which case $M \to \infty$ at the equator). However, since K_M is conserved throughout the evolution, the time-dependent solutions of the total angular-momentum-conserving model are characterized by unphysically large oscillations about the mean state that dominate the solution in the absence of dissipation and lead to instability.

c. Convective heat sources

The inclusion of convective heat sources into the SWM is obtained by associating high-level divergence with latent heat release (i.e., a mass source) and, conversely, high-level convergence (coupled to low-level divergence) with a mass sink, as described in Held and Phillips (1990). This implies an additional source term in Eq. (2c):

$$Q_C = \kappa V', \tag{29}$$

where κ is a positive humidity function. The only effect this addition has on the two steady states is a correction to V in the uniform-M steady state:

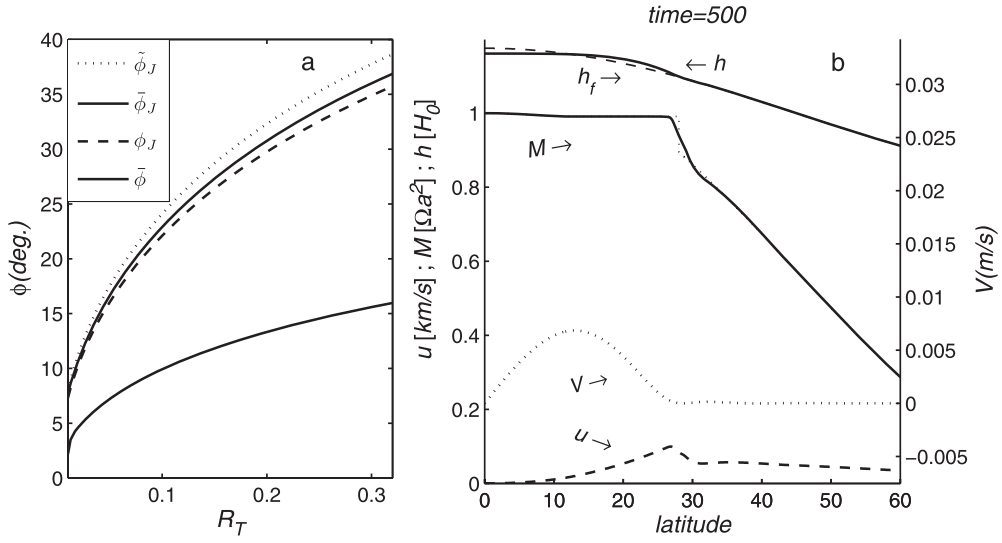

FIG. 9. (a) The approximate solution for $\tilde{\phi}_J$ (dotted) corresponding to $\tilde{\mu}_J = \sqrt{2R_T/(1+2R_T)}$ and the approximate $\bar{\phi}_J$ and $\bar{\phi}$ corresponding to the $\bar{\mu}_J$ and $\bar{\mu}$ roots of Eqs. (26a) and (26b), respectively (both solid but $\bar{\phi}_J > \bar{\phi}$) and ϕ_J of the exact $M_0 = 1$ contour of Fig. 7 (dashed). (b) Near-steady state of the 1½-layer model at $t = 500$ for the parameters $\alpha_g = 18\tau^2$, $\alpha_\tau = (2\pi\tau)^2$, and $h_1 = 0.175$ ($R_T = 0.16$; $\tau = 20$ days) and the initial conditions [(11a)–(11c)]; h_f is shown for reference in dashed gray; $M(\mu)$ is approximated using Eqs. (26a) and (26b) and the three-region paradigm (dotted, gray) is distinguishable from M given by the solution of the time-dependent equations only at the transition region. The dimensional scales for the height (H_0, top solid), the forcing height (top dashed gray), M (Ωa^2, solid), and the zonal velocity u (1 km s^{-1}; dotted), are given on the left ordinate while the dimensional scale for V (m s^{-1}; dashed) is given on the right ordinate. The angular momentum structure clearly shows the formation of three steady-state regions in the 1½-layer model: a tropical, mass acquiring, region ($0 < \mu < \bar{\mu}$), a subtropical, mass depleting, uniform-M region ($\bar{\mu} < \mu < \mu_T$), and an extratropical radiative-equilibrium region ($\mu_T + \Delta\mu < \mu$). The latter region is connected to the uniform-M region by an unsteady transition region: $\mu_T < \mu < \mu_T + \Delta\mu$. The meridional axis is truncated at 60°, poleward of which radiative equilibrium is fully established at the indicated time.

$$V = -\frac{\int (h - h_f + V\kappa')d\mu}{h - \kappa}. \tag{30}$$

$$\Delta K^A_{Vh} = \kappa \int_0^{\mu_J} \left[\int_0^{\mu} (h_f/h - 1)d\mu' \right] d\mu, \tag{31}$$

Under terrestrial conditions we may assume $\mathrm{sgn}(V\kappa') < 0$. In addition, for $\kappa = h$ Eq. (30) becomes singular. Therefore, for $\kappa < h$ the incorporation of moisture as a possible source/sink of heat via the divergence of V does not incur a loss of generality to the attractor set other than the intensification of V [whose square remains negligible in Eq. (7c), not affecting the approximate expressions for the steady states]. This result is a specific SWM case of the more general heat sources, discussed by HH80 and Hou and Lindzen (1992), in which $\int_0^{\mu_J} Q_C d\mu = 0$ is satisfied. Using Eqs. (29) and (30), it follows that, for a constant κ and approximating a uniform h at the equator, a state in which the convective forcing approximately equals the radiative forcing at the equator corresponds to $\kappa \approx$ ½. In the case $\kappa = \text{const} \ll 1$, the correction to the circulation strength approximately equals where ΔK^A_{Vh} denotes the convective contribution to the circulation strength.

To sum up the results of this section: The physically favored interpretation of the forcing term in system (2) is that it represents a source of mass (and not heat) injected into the active layer from the underlying passive bottom layer. As predicted by HH80, the introduction of moisture into the present model (proportional to ∇V) intensifies the circulation's strength but does not alter the extent of the tropical cell.

5. Summary and discussion

The use of angular momentum as a dynamical variable in system (2) yields the simple Eq. (2b) that replaces Eq. (1b) and immediately identifies the system's only two steady states: radiative equilibrium and uniform-M.

The hemispheric symmetry of the problem leaves M_0 (the angular momentum at the equator) unchanged (i.e., set by the initial conditions). The two equinoctial steady states of system (2) can therefore be reached only if the value of M_0 equals the value of M associated with either the radiative equilibrium ($= \sqrt{1 + 2R_T}$) or the uniform-M ($= 0$) steady state. All other (positive) values of M at the equator will lead to a near-steady state made up of a tropical uniform-M region, an extratropical radiative-equilibrium region, and an ever-narrowing, unsteady transition region. The long-time behavior of system (2) is the convergence to an attractor set, fully described by $[\mu_J(M_0, R_T), M_0, R_T]$, whose basin of attraction has a one-dimensional representation using the basin number $B_E = M_0^2/(1 + 2R_T)$. It is possible to introduce the effect of convective heat sources into the SWM by associating divergence/convergence with a heat source/sink (Held and Phillips 1990). As discussed in section 4c, in general this additional source term does not affect qualitatively the long-time behavior of system (2) other than the intensification of V.

The geometric simplicity of the basin of attraction (found in section 3d) results directly from the hemispheric symmetry of the heating. This simple geometry is expected to change drastically when the hemispheric symmetry is broken, for example, by off-equatorial heating ($\mu_0 \neq 0$). It is also not clear whether such a simple geometry exists in axially symmetric two-dimensional (latitude, height) models since very little attention has been given in previous studies (e.g., HH80; Lindzen and Hou 1988) to the dependence of the steady states on the initial conditions, so the possibility of multiple attractor sets was not studied.

In viscous two-dimensional (latitude, height) axially symmetric models (e.g., the HH80 model) Hide's theorem mandates that M be everywhere ≤ 1 that is, $u \leq 1$ $\sin^2(\phi)/\cos(\phi)$. HH80 theory is a particular case [where $M = 1$, so $u(0) = 0$)] of a broader set of solutions of the forced SWM in which states with $M \leq 1$ as well as $M > 1$ are allowed at the equator, as shown in Fig. 7.

In a 1½-SWM where the mass source is assumed to be a stationary bottom layer (that injects the mass of fluid with zero relative momentum) and for physically acceptable initial conditions, the steady states of the present SWM were found to be independent of the initial conditions. These steady states prohibit nonvanishing zonal velocities on the equator (i.e., they yield restrictions similar to those of Hide's theorem). The attractor set of this 1½-SWM is completely determined by the value of R_T and consists of three regions: a tropical, mass acquiring region in which h is nearly uniform, a subtropical uniform-M region, and an extratropical radiative-equilibrium region. The analytical solutions of this three-region paradigm are in better agreement with the numerical results of HH80 and Walker and Schneider (2006) than the SWM. The main reason for this improved agreement is that the 1½-SWM has intermediate local Rossby numbers in the tropics, with $0 < \mathrm{Ro} = (1 + M'/2\mu) \leq 1$ (or $\mathrm{Ro} = -\zeta/f$ in dimensional form, where ζ is the relative vorticity), whereas the SWM only supports $\mathrm{Ro} = 1$ (i.e., $M' = 0$) there.

The interpretation of the source term as a mass source is reaffirmed by contrasting the 1½-SWM with an angular momentum–conserving model in which the source term represents a heat source where the solutions were found to be physically unrealistic.

The assumption of a nearly uniform-h tropical region used to obtain approximate accurate solutions of the 1½-SWM is in agreement with the adaptation of the weak temperature gradient (WTG) approximation to the shallow-water equations. As was shown by Polvani and Sobel (2002), the WTG approximation agrees well with the SWM only for $M_0 \approx 1$ and, as predicted by Schneider (2006), this approximation is accurate only in the mass acquiring region of the 1½-SWM.

The state of the system at different times is easily described using the profile of the angular momentum, which is discontinuous in the attractor sets of the SWM and the 1½-SWM. The ubiquity of discontinuous solutions in equations such as (2a) suggests that spectral methods are inappropriate for long integrations since these methods suppress discontinuous solutions crucial to the understanding of the dynamics.

It was reaffirmed here that, as in viscous models, steady states of the SWM are reached after times much longer than a season. If time-dependent forcing with a period on the order of a season is applied, the system can be expected to always be in a transient state, which limits the applicability of predictions based on steady-state theories (including Hide's theorem). The calculations of Fang and Tung (1999), however, demonstrate that, for forcing in which the locus of the maximal heating is allowed to simulate seasonal variations, the steady solutions are in good qualitative agreement with the time-dependent solutions. Thus, while near-steady states are reached at times that exceed a season, the solutions for the attractor sets of the SWM and 1½-SWM presented in Figs. 7 and 9, respectively, and the total mass fluxes presented in Fig. 8 provide a concise qualitative tool for predicting the axisymmetric dependence of the subtropical jets and the circulation strength on parameters such as the earth's radius, rotation rate, and differential heating.

Acknowledgments. This study was supported by the Israel Science Foundation via Grant 579/05 to HU. OA

thanks the Eshkol foundation for providing the Ph.D. Candidate Fellowship. We are also grateful to three anonymous reviewers whose suggestions helped us improve the presentation of the fine points of this work. This study is part of OA's Ph.D. dissertation at HU.

REFERENCES

Ambaum, M., 1997: Isentropic formation of the tropopause. *J. Atmos. Sci.,* **54,** 555–568.

Déqué, M., and D. Cariolle, 1986: Some destabilizing properties of the Asselin time filter. *Mon. Wea. Rev.,* **114,** 880–884.

Dvorkin, Y., and N. Paldor, 1999: Analytical considerations of Lagrangian cross-equatorial flow. *J. Atmos. Sci.,* **56,** 1229–1237.

Emanuel, K. A., 1995: On thermally direct circulations in moist atmospheres. *J. Atmos. Sci.,* **52,** 1529–1534.

Esler, J. G., L. M. Polvani, and R. A. Plumb, 2000: The effect of a Hadley circulation on the propagation and reflection of planetary waves in a simple one-layer model. *J. Atmos. Sci.,* **57,** 1536–1556.

Evans, L. C., 1998: *Partial Differential Equations*. American Mathematical Society, 662 pp.

Fang, M., and K. K. Tung, 1996: A simple model of nonlinear Hadley circulation with an ITCZ: Analytic and numerical solutions. *J. Atmos. Sci.,* **53,** 1241–1261.

——, and ——, 1997: The dependence of the Hadley circulation on the thermal relaxation time. *J. Atmos. Sci.,* **54,** 1379–1384.

——, and ——, 1999: Time-dependent nonlinear Hadley circulation. *J. Atmos. Sci.,* **56,** 1797–1807.

Gill, A. E., 1982: *Atmosphere–Ocean Dynamics*. Academic Press, 645 pp.

Held, I. M., and A. Y. Hou, 1980: Nonlinear axially symmetric circulations in a nearly inviscid atmosphere. *J. Atmos. Sci.,* **37,** 515–533.

——, and P. J. Phillips, 1990: A barotropic model of the interaction between the Hadley cell and a Rossby wave. *J. Atmos. Sci.,* **47,** 856–869.

Hoskins, B. J., M. E. McIntyre, and A. W. Robertson, 1985: On the use and significance of isentropic potential vorticity maps. *Quart. J. Roy. Meteor. Soc.,* **111,** 877–946.

Hou, A. Y., and R. S. Lindzen, 1992: The influence of concentrated heating on the Hadley circulation. *J. Atmos. Sci.,* **49,** 1233–1241.

Lee, S., 1999: Why are the climatological zonal winds easterly in the equatorial upper troposphere? *J. Atmos. Sci.,* **56,** 1353–1363.

LeFloch, P. G., 2002: *Hyperbolic Systems of Conservation Laws: The Theory of Classical and Nonclassical Shock Waves*. Birkhäuser Basel, 294 pp.

Lindzen, R. S., and A. Y. Hou, 1988: Hadley circulations for zonally averaged heating centered off the equator. *J. Atmos. Sci.,* **45,** 2416–2427.

Lorenz, E. N., 1967: *The Nature and Theory of the General Circulation of the Atmosphere*. WMO, 161 pp.

Paldor, N., 2001: The zonal drift associated with time-dependent particle motion on the earth. *Quart. J. Roy. Meteor. Soc.,* **127,** 2435–2450.

——, 2002: The transport in the Ekman surface layer on the spherical Earth. *J. Mar. Res.,* **60,** 47–72.

Plumb, R. A., and A. Y. Hou, 1992: The response of a zonally symmetric atmosphere to subtropical thermal forcing: Threshold behavior. *J. Atmos. Sci.,* **49,** 1790–1799.

Polvani, L. M., and A. H. Sobel, 2002: The Hadley circulation and the weak temperature gradient approximation. *J. Atmos. Sci.,* **59,** 1744–1752.

Satoh, M., 1994: Hadley circulations in radiative–convective equilibrium in an axially symmetric atmosphere. *J. Atmos. Sci.,* **51,** 1947–1968.

Schlesinger, R. E., L. W. Uccellini, and D. R. Johnson, 1983: The effects of the Asselin time filter on numerical solutions to the linearized shallow-water wave equations. *Mon. Wea. Rev.,* **111,** 455–467.

Schneider, E. K., 1977: Axially symmetric steady-state models of the basic state for instability and climate studies. Part II. Nonlinear calculations. *J. Atmos. Sci.,* **34,** 280–296.

——, and R. S. Lindzen, 1977: Axially symmetric steady-state models of the basic state for instability and climate studies. Part I. Linearized calculations. *J. Atmos. Sci.,* **34,** 263–279.

Schneider, T., 2006: The general circulation of the atmosphere. *Annu. Rev. Earth Planet. Sci.,* **34,** 655–688.

Shell, K. M., and I. M. Held, 2004: Abrupt transition to strong superrotation in an axisymmetric model of the upper troposphere. *J. Atmos. Sci.,* **61,** 2928–2935.

Walker, C. C., and T. Schneider, 2005: Response of idealized Hadley circulations to seasonally varying heating. *Geophys. Res. Lett.,* **32,** L06813, doi:10.1029/2004GL022304.

——, and ——, 2006: Eddy influences on Hadley circulations: Simulations with an idealized GCM. *J. Atmos. Sci.,* **63,** 3333–3350.

Williams, G. P., 2003: Jet sets. *J. Meteor. Soc. Japan,* **81,** 439–476.